Tribology Letters (2018) 66:156
https://doi.org/10.1007/s11249-018-1108-9

ORIGINAL PAPER

Graphene Nanoplatelet (GNP)-Incorporated AZ31 Magnesium Nanocomposite: Microstructural, Mechanical and Tribological Properties

M. Arab[1] · **S. P. H. Marashi**[1]

Received: 20 August 2018 / Accepted: 23 October 2018

Abstract
Graphene nanoplatelets (GNPs), despite their unique properties, were not widely investigated as reinforcement in metal matrix nanocomposites. The nanocomposite was fabricated by adding 15-nm-thick GNPs to AZ31 magnesium alloy via friction stir processing (FSP). Mechanical, frictional and wear properties were investigated. It was observed that refined microstructure with a range of 3–9 μm grain size and the presence of GNPs, i.e., reinforcing particles, improved the tensile properties and increased the ultimate tensile strength to 278 MPa. FSP increased the strain-to-fail by 133% compared to that of base metal, while it was decreased by adding GNPs. Moreover, the presence of GNPs decreased the adhesive wear mechanism by squeezing out, smudging on the surface and, finally, forming a protective layer between the sliding surfaces. Hence, the coefficient of friction was decreased to 60% and the range of fluctuations in friction plot was confined by adding GNPs. They were further decreased by increasing the normal load and sliding velocity due to easier debonding of the GNPs and the surrounding AZ31 Mg matrix resulting in forming a lubricating layer between sliding surfaces.

Keywords AZ31 Mg alloy · Graphene nanoplatelets (GNPs) · Self-lubricating nancomposite · Friction stir processing (FSP) · Self-lubrication friction · Tribological properties

1 Introduction

Magnesium (Mg) is considered as an attractive metal due to its high stiffness and specific strength as well as low density. It can be used in innovative improvements in light-weight structural applications, especially in transportation industry [1, 2]. Indeed, one of the best candidates to justify these growing demands is unprecedented types of Mg-based composites [3, 4]. However, some weak properties of Mg alloys and compounds, such as poor wear and corrosion resistance, need to be improved prior to utilization [3]. Using new composite reinforcements, including nanoscale particles, can help overcome these limitations [5].

Stably isolated graphene, since the discovery by Novoselov in 2004 [6], has been at the centre of attentions from bench researches to professional applications due to its unique properties [5, 7]. Graphene is an atomically smooth two-dimensional material which acts as a highly impermeable layer to some gases, which can slow down the oxidative and corrosive phenomena, and as a result, ameliorate the wear resistance [8]. Defect-free graphene sheet shows an extreme mechanical strength of around 1 TPa of Young's modulus (E), which is desirable for mechanical strengthening and wear protection [9]. Furthermore, it acts as a thin solid film which can reduce the friction between sliding surfaces [10]. The above-mentioned properties make graphene a proper candidate for demanding tribological uses to achieve better wear regimes and lower friction [11].

Improved mechanical and tribological properties together with significant microstructural refinement can be achieved by friction stir processing (FSP) as one of the severe plastic deformation (SPD) processes [12]. Numerous investigations have demonstrated that FSP can improve tribological properties of Mg-based composites using proper reinforcing particles [12, 13].

✉ S. P. H. Marashi
pmarashi@aut.ac.ir

M. Arab
mohsen.arab@aut.ac.ir

[1] Department of Mining and Metallurgical Engineering, Amirkabir University of Technology, P.O. Box 15875-4413, Tehran, Iran

Published online: 08 November 2018

Table 1 Chemical composition of AZ31 Mg alloy

Mg alloy	Chemical composition (wt %)					
	Al	Zn	Mn	Ca	S	Mg
AZ31	2.53	1.27	0.13	0.014	0.011	Bal

There have been few researches on graphene-reinforced Mg matrix composites [14]. The first report was published in 2012 by Chen et al. [15] in which liquid-state ultrasonic processing and solid-state FSP were employed to fabricate nanocomposite. It was reported that the fabrication method was an effective way to disperse graphene nanoplatelets (GNPs) into the Mg matrix in which the microhardness of 1.2 vol% GNP-reinforced specimen was reported to be 78% more than that of pure Mg. Rashad et al. [16–18] investigated some aspects of graphene-reinforced Mg-based composite fabricated by semi-powder metallurgy followed by hot extrusion. The addition of GNPs increased the yield strength (YS), ultimate tensile strength (UTS), and ductility for Mg/(10 Ti–0.18 GNPs) composite [16]. For Mg/0.3 wt% GNPs composite, the hardness, YS, and UTS were 68.5 HV, 197 MPa, and 238 MPa, respectively [17]. For Mg/(1% Al–1% Sn–0.18% GNPs) composite, YS and UTS were 208 and 269 MPa which were increased by 29.2% and 14%, respectively, compared to that of pure Mg [18]. The improvement of mechanical properties proves the positive effect of GNPs. They reported that the hardness, YS, and fracture strain were increased by increasing the GNPs content.

Among various applications of GNPs, tribological applications are still the least explored. In the present study, GNP-incorporated AZ31 Mg nanocomposite was fabricated by FSP in order to take the advantage of the extremely high wear resistance properties of GNPs while still remaining a light-weight Mg alloy. Wear tests were conducted by a pin-on-disc setup under dry sliding condition having a constant sliding distance of 1000 m in the normal load range of 5–20 N and a sliding velocity range of 0.2–1.25 m/s.

The aim of this study is to develop the understanding of the factors controlling the tribological properties of AZ31/GNPs Mg composite in order to provide an analytical basis for the evaluation of the wear behaviour and mechanisms in different wear conditions. In order to do so, at first, variations of microstructural and mechanical properties are presented; then, the features of friction curve consisting of fluctuations, coefficient of friction (COF) and wear mechanisms are discussed. Finally, the effect of GNPs on wear properties is investigated in each part.

2 Materials and Methods

The chemical composition of the AZ31 Mg alloy as the base metal (BM) is shown in Table 1. The GNPs, dry powder with the specifications presented in Table 2, were purchased from XG Sciences Company, Lansing, MI, USA [19]. Field emission scanning electron microscopy (FESEM) image of GNPs, using secondary electrons with 15 kV accelerating voltage and 4 mm working distance, is shown in Fig. 1a. Moreover, the transmission electron microscopy (TEM) image of the GNPs, provided by the manufacturing factory [19], is shown in Fig. 1b. Cubic specimens having dimensions of $100\times50\times5$ mm^3 were prepared from Mg alloy sheet. Afterwards, a groove with dimensions of $100\times3\times2$ mm^3, as shown in Fig. 2, was wire cut 0.5 mm below the surface. The groove was filled up with GNPs. The profile structure kept the GNPs in the groove during the FSP.

FSP was carried out by a computer numerical control (CNC) equipment using an especially designed FSP fixture and H13 tool steel. The FSP tool was a commonly used threaded tapered with 18 mm shoulder diameter, 4 mm pin length and 6 and 5 mm the larger and smaller diameters of the pin, respectively. An optimized set of FSP parameters comprises 700 rpm tool rotational speed, 90 mm/min linear speed, 0.3 mm plunge depth and 3 degrees tilt angle. Two FSP passes were used in the current study.

Specimens were sectioned perpendicular to the processing direction for microstructural studies. The microstructural specimens were prepared based on metallographic procedure according to the ASTM E3 standard [20] and etched by a solution including 10 ml of acetic acid, 6 g of picric acid, 10 ml of water and 100 ml of ethanol for 10 s. The optical microscopy (OM) analysis was used for microstructural study; then, the average grain size was determined based on the ASTM E112 standard [21].

Mechanical properties were determined using microhardness and tensile tests. Microhardness measurements were performed by Schimadzu type M. It was measured along the

Table 2 Characterization of GNPs [19]

GNPs	Properties			
	Thickness (nm)	Diameter (μ)	Surfacearea(m^2/g)	Density (g/cm^3)
H-15	15	15	50–80	0.03–0.1

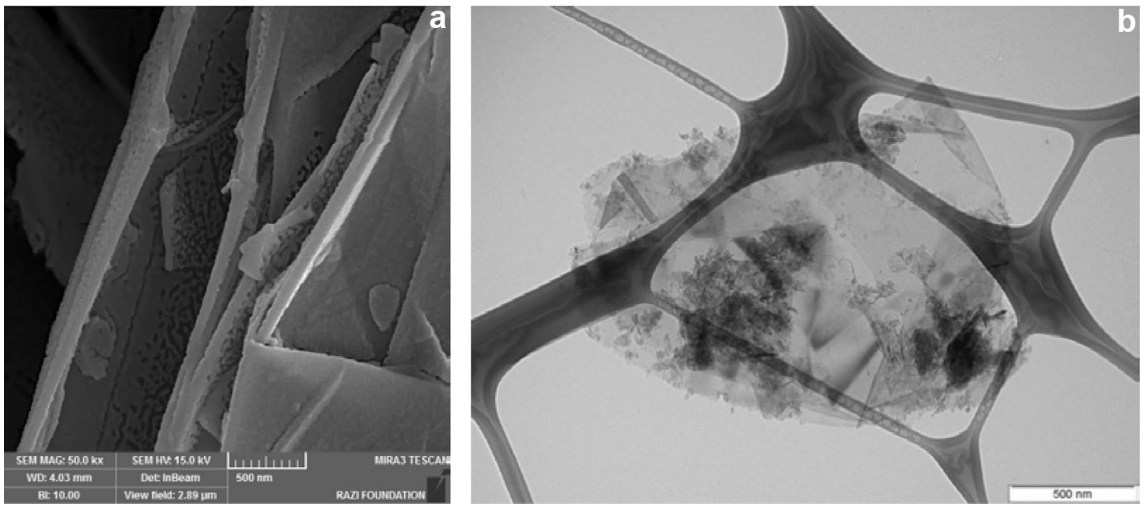

Fig. 1 FESEM (**a**) and TEM [19] (**b**) images of H15 GNPs

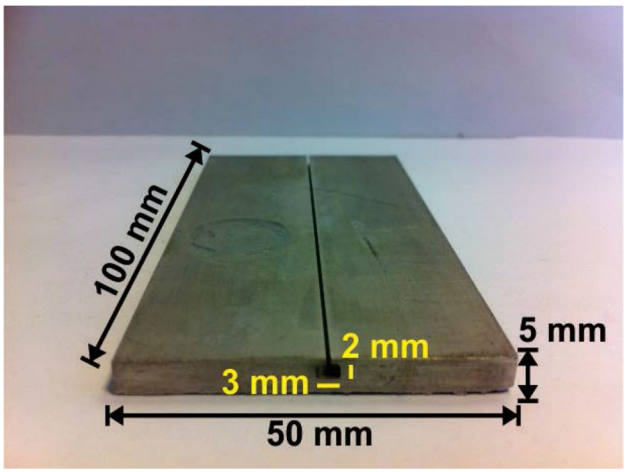

Fig. 2 Dimensions of the strip with the wire cut groove

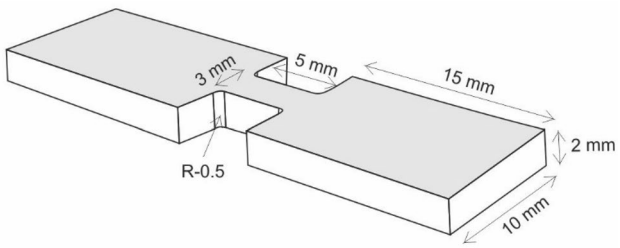

Fig. 3 Dimensions of dog-bone tensile test specimen

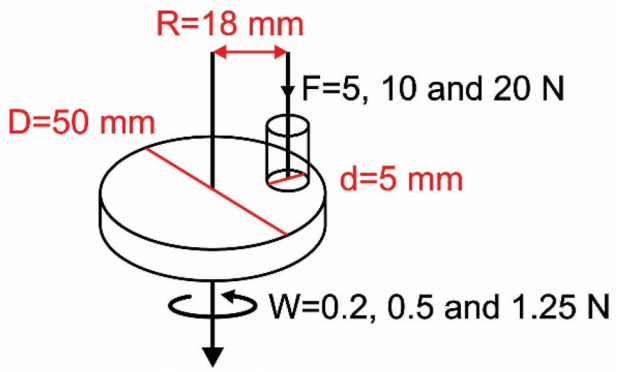

Fig. 4 Schematic illustration of pin-on-disc test in which F is the normal load on the pin, d is the pin diameter, D is the disc diameter, R is the track radius and W is the sliding velocity of the disc

cross section at 0.5-mm distance from the top surface using a Vickers microhardness method according to the ASTM E384 standard [22] by applying a load of 100 gf for 10 s. The tensile test procedure was carried out at ambient temperature using an initial strain rate of 1×10^{3} s^{1} by means of Santam STM20 testing machine with the maximum load of 10 kN. The dog-bone flat specimen with the gauge dimensions of $5\times3\times2$ mm^{3}, shown in Fig. 3, was cut parallel to the FSP direction, with stirred zone (SZ) being centred within the gauge length by an electric discharge machining (EDM). They were mechanically grounded by abrasive papers before wire cut.

Dry sliding wear test was performed using a standard pin-on-disc test machine based on ASTM G99 standard [23] at room temperature, as proposed in Fig. 4. Circular pin of 5 mm diameter was cut from the SZ of the as-processed specimens for the wear tests by the EDM, with the axis of the pins perpendicular to the FSP direction. AISI 52,100 steel discs with 50 mm diameter, 6 mm thickness, hardness of about 55 HRC and arithmetic average roughness of 0.15 µm were used as the counter face material. Care must be taken in pin and disc preparation to avoid subsurface

damages that alters the wear results, significantly. All wear tests were conducted at normal loads of 5, 10 and 20 N under three sliding velocities of 0.2, 0.5 and 1.25 m/s for 1000-m sliding distance. The wear track radius on the disc surface was 18 mm. Weight loss of test specimen was measured. Lower weight loss indicates better wear resistance. Before and after each test, both disc and specimen were cleaned by ethanol and dried in the air in order to avoid contaminations. The worn surfaces of the samples were examined by field emission scanning electron microscopy (FESEM) equipped with energy dispersive spectroscopy (EDS) using backscattered electrons with 15 kV accelerating voltage, 12.35 ± 0.20 mm working distance and 10 nA beam current.

3 Results and Discussions

3.1 Microstructural Evaluations

Figure 5 illustrates the cross-sectional macroimage of the GNP-incorporated specimen. Both dimensions and shape of the processing region are relatively the same for all FSPed specimens, because of the constant FSP parameters including traverse and rotational speeds, the number of FSP pass and the frictional heat generation which are the main effective parameters [24].

Figure 6a–c shows the microstructure of base material (BM), conventional FSP and GNP-incorporated specimens, respectively. The OM micrograph of the BM specimen, shown in Fig. 6a, exhibits a bimodal microstructure which is mainly composed of coarse α-Mg grains (~ 55.3 μm) together with some fine grains (~ 10.2 μm) consistently distributed in the matrix. The microstructure of SZ of conventional FSP specimen is rather characterized by some highly deformed grains alongside fine recrystallized grains, shown in Fig. 6b. The formation of coarser grains is due to more heat generated by the friction between the tool shoulder and the surface of specimen [25]. The microstructure of the SZ of GNP-incorporated specimen, shown in Fig. 6c, illustrates equiaxed and fully recrystallized grain distribution. It shows refined structure with a range of 3–9 μm grain size. This implies the Zener pinning effect of GNPs which intensifies the effect of FSP on grain refinement.

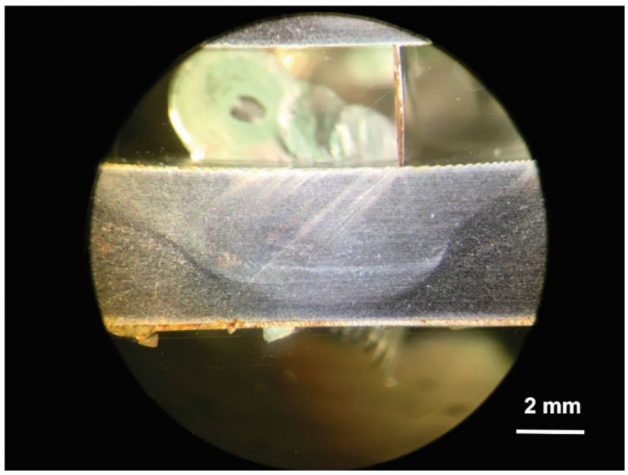

Fig. 5 Cross-sectional macroimage of GNP-incorporated specimen

3.2 Microhardness Investigations

The microhardness values of the BM specimen as well as its variations for the conventional FSP and GNP-incorporated specimens are shown in Fig. 7. As mentioned in Table 3, the average microhardness of the BM specimen is 56 HV which was increased by FSP to 64 HV. It was considerably increased to around 79 HV by adding GNPs. Grain boundary strengthening in accordance with well-known Hall–Petch equation and Zener pinning effect of GNPs on the movement of low- and high-angle grain boundaries are believed to be the major phenomena that contributed in enhancing the microhardness value of the GNP-incorporated specimen.

3.3 Tensile Properties

The engineering stress–strain curves for the BM, conventional FSP and GNP-incorporated specimens are shown in Fig. 8. The YS, UTS and strain-to-fail values of tensile tests are listed in Table 3. It can be noticed that strain-to-fail of conventional FSP specimen is increased by 2.3 times compared to that of the BM specimen, while it is decreased to 15.8% by adding GNPs. Moreover, the YS and UTS values of GNP-incorporated specimen are increased to 217 and 278 MPa, respectively. In fact, the mechanical properties were just slightly increased compared to those of the BM specimen.

Under tensile loading condition, the load is transferred from strained matrix to reinforcement particles through shear stress that exists at the matrix–reinforcement interface. Therefore, the reinforcements help to resist against fracture. In randomly distributed GNPs in Mg matrix, the GNPs that are aligned along tensile direction are further strained under tensile loading and contribute in improvement of the mechanical properties of nanocomposite [26]. Therefore, load transfer from soft Mg matrix to strong GNPs is one of the most important strengthening effects of GNPs in the nanocomposite which is revealed in Fig. 8 and Table 3. However, weak interface limits the strengthening effect of GNPs on improvement of tensile properties. Crack nucleation in the weak interface limits the strain-to-fail.

The mismatch in coefficient of thermal expansion between Mg ($CTE = 26 \times 10^{-6}\ K^{-1}$) and GNPs ($CTE = 1 \times 10^{-6}\ K^{-1}$) may lead to the generation of dislocations in the

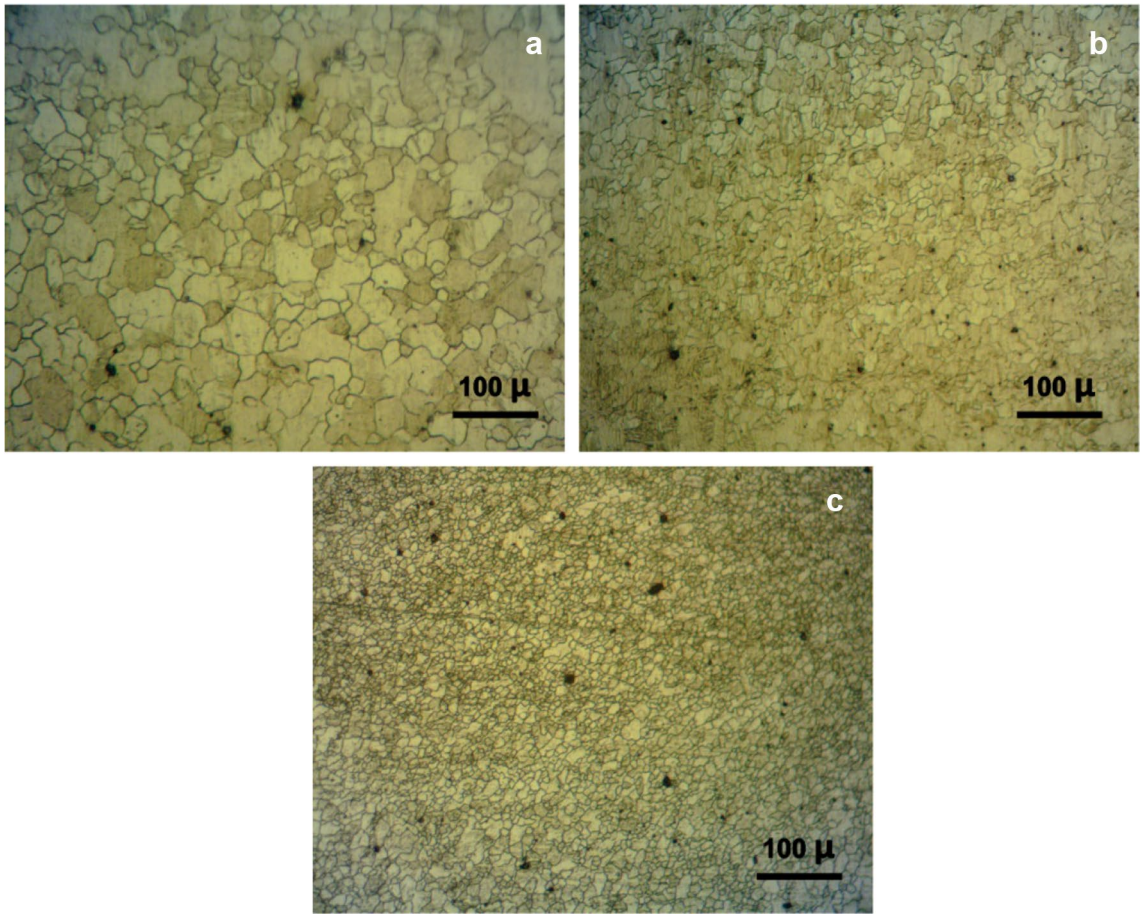

Fig. 6 OM micrographs of the BM (**a**), conventional FSP (**b**) and GNP-incorporated (**c**) specimens

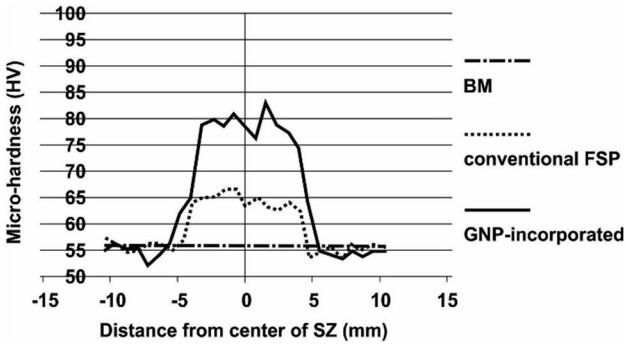

Fig. 7 Microhardness profile of the BM, conventional FSP and GNP-incorporated specimens

matrix–reinforcement interface [27, 28]. The generation of dislocations is another possible reason for better mechanical properties of nanocomposite. The other strengthening mechanism for GNPs embedded in the matrix is the Orowan looping [7]. Residual dislocation loops may form around GNPs after a dislocation bows out and bypasses them. High work hardening rate can be resulted from these loops.

Table 3 Values of mechanical properties

Specimen name	Vickers hardness (HV)	YS (MPa)	UTS (MPa)	Strain-to-fail (%)
BM	56	215	256	13.3
conventional FSP	64	138	208	31.1
GNP-incorporated	79	217	278	15.8

3.4 Tribological Analysis

The variations of COF for the BM and conventional FSP specimens are plotted against sliding distance in Fig. 9a, b, respectively, under 10 N normal load and 0.5 m/s sliding velocity. The same plots are represented for the GNP-incorporated specimens, under different normal loads and sliding velocities at full combination of 5, 10 and 20 N normal loads and 0.2, 0.5 and 1.25 m/s sliding velocities depicted in Fig. 10.

The reported COF value is the arithmetic mean of experimental data recorded for each specimen. The COF values of

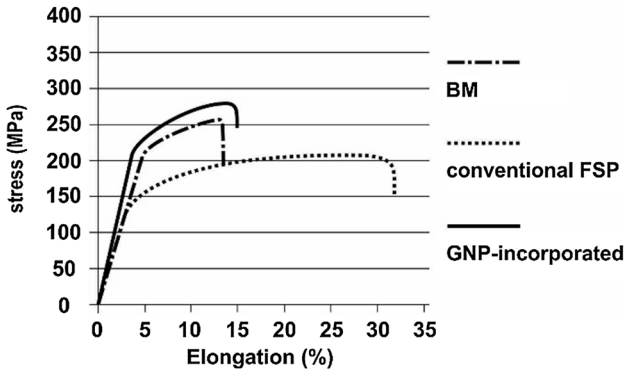

Fig. 8 Stress–strain curves for the BM, conventional FSP and GNP-incorporated specimens

GNP-incorporated specimens, related to Fig. 10, are listed in Table 4. It is around 0.5 for the BM specimen.

High fluctuations in the COF curve is one of the consequences of severe adhesive wear mechanism. The widest range of fluctuations belongs to the BM specimen. In fact, the accumulation and elimination of wear debris on the worn tracks of surface [29] and local adhesion and detachment of pin and disc surfaces [30] cause high fluctuations in the friction plot. An increase in the normal load results in an increase in the local frictional heat and the adhesion of sliding surfaces, which as a result intensifies the intensity of fluctuations. However, the intensity of fluctuations is almost constant despite increasing the normal load for GNP-incorporated specimens, as shown in Fig. 10. This phenomenon may have two possible reasons. First, high normal load not only reduces the abrasion by grinding wear debris and reducing their destructive effects, but also prevents the accumulation of wear debris on the of surface worn tracks. Second, an increase in the normal load can increase the local temperature, which as a result increases the oxidation of sliding surfaces and diminishes the adhesive wear mechanism. The sliding surfaces are covered by oxides formed by repeated sliding motion of the surfaces and wear debris which is called oxidative wear mechanism. Higher sliding velocity helps the entrapped wear debris gaining sufficient outward thrust to get out of the interacting surfaces. In this situation, metal wear debris, due to greater weight than the GNPs, gain more gravitational acceleration and get out of the interacting surfaces quickly. Thus, lower amount of harsh metal debris reduces the intensity of abrasive wear. In addition, GNPs decrease the adhesion of surfaces and, subsequently, diminish the intensity of fluctuations by forming a self-lubricating layer between the sliding surfaces. Thus, wear resistance is improved constantly by increasing the sliding velocity, due to more amount of remained GNPs in wear debris compared to the harsh metal wear debris, as shown in Figs. 9 and 10.

Fewer damages can be seen on the disc surface compared to magnesium composite pin due to its higher hardness. In wear condition of low normal load and sliding velocity, severe adhesive and abrasive wear mechanisms are the main reasons of reducing the weight of disc. On the other hand, by increasing normal load and sliding velocity, plastic deformation, which is one of the main mechanisms of wear, appears due to an increase in local temperature and applied force. In this wear test condition, the wear debris stick to the disc surface and increase the weight of the disc. It can be concluded that the disc weight variations are heavily dependent on wear mechanisms and frictional temperature. These are consistent with the above-mentioned fluctuations in the COF curve and wear damages.

Figure 11 shows the COF values of GNP-incorporated specimen as a function of sliding velocity at different normal loads. It can be observed that the COF values are reduced at higher normal loads and sliding velocities. Some other researchers have also reported the same trend for COF values [31].

The descending trend of the COF value may be attributed to two main possible reasons. First, increasing the local frictional heat leads to an increase in the probability of surface oxidation. Second, the GNPs have two possible effects on improvement of wear resistance. The first effect was revealed by the backscattered electron (BSC) images and the energy

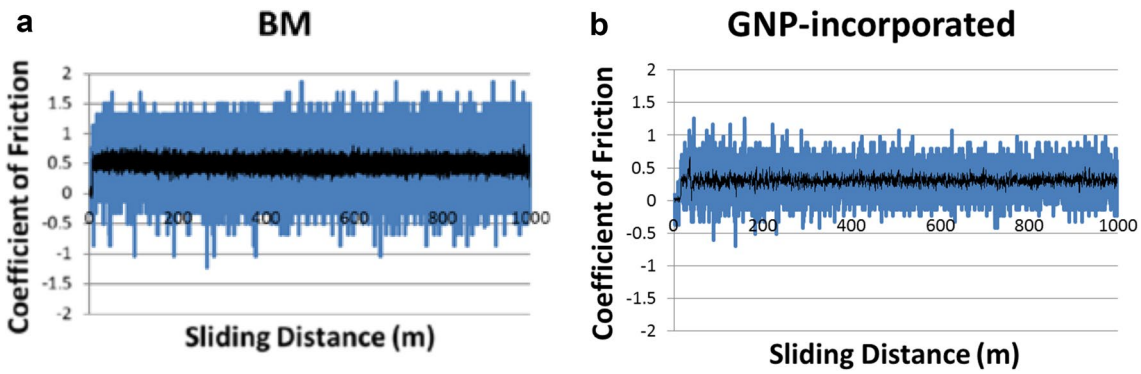

Fig. 9 Friction plots for BM (**a**) and GNP-incorporated, (**b**) specimens at 10 N normal load and 0.5 m/s sliding velocity

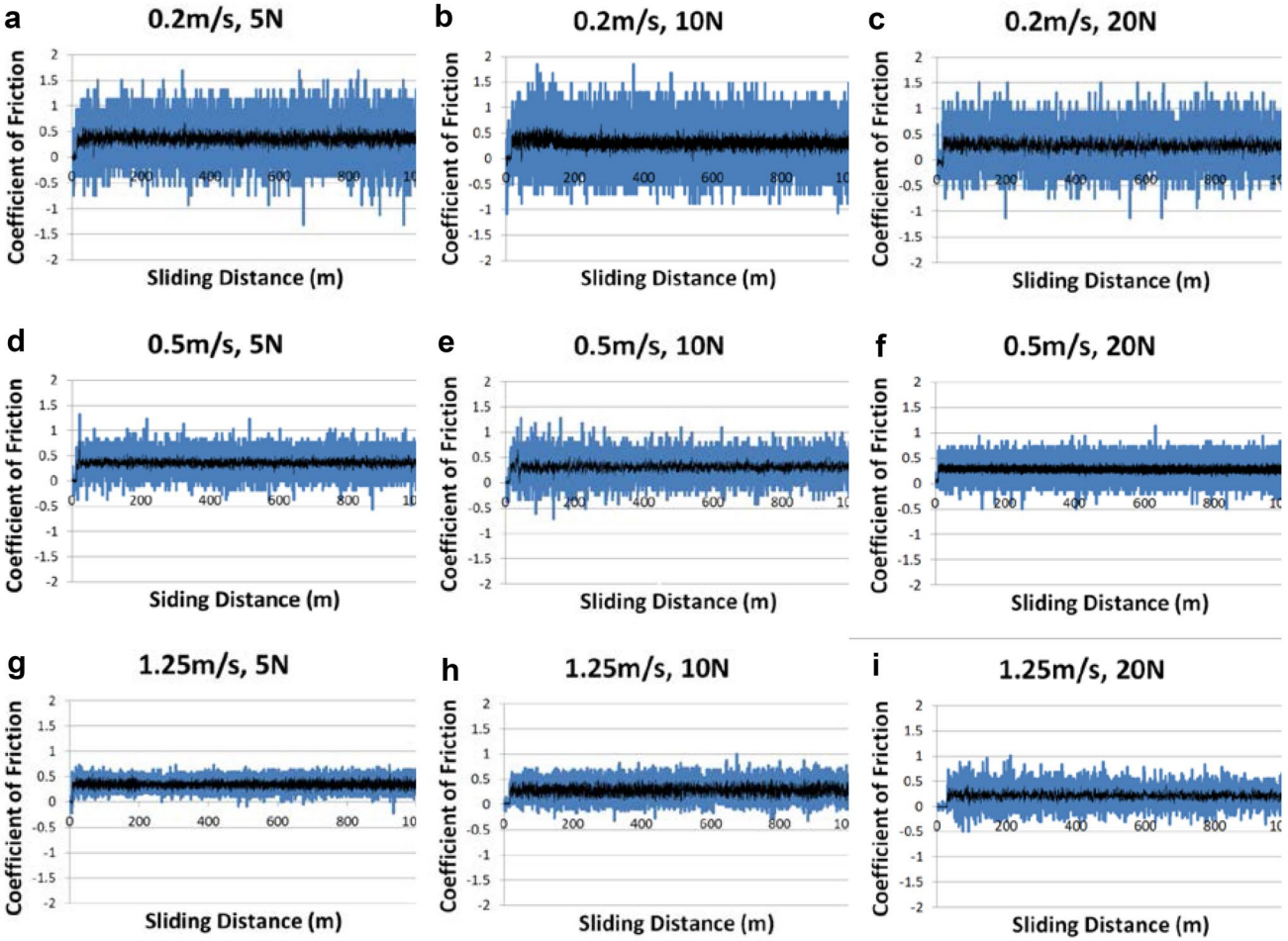

Fig. 10 Friction plots for AZ31/GNPs Mg composite at 5 N and 0.2 m/s (**a**), 10 N and 0.2 m/s (**b**), 20 N and 0.2 m/s (**c**), 5 N and 0.5 m/s (**d**), 10 N and 0.5 m/s (**e**), 20 N and 0.5 m/s (**f**), 5 N and 1.25 m/s (**g**), 10 N and 1.25 m/s (**h**) and 20 N and 1.25 m/s (**i**) normal load and sliding velocity, respectively

Table 4 COF values related to Fig. 10

AZ31/GNPs Mg nano-composite		Sliding velocity (m/s)		
		0.2	0.5	1.25
Normal load (N)	5	0.36	0.30	0.28
	10	0.35	0.34	0.27
	20	0.34	0.28	0.20

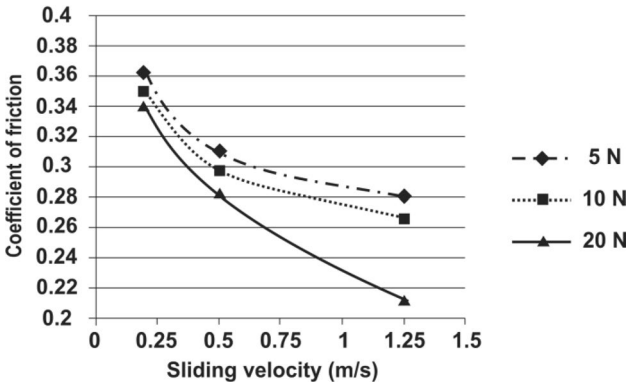

Fig. 11 COF values versus sliding velocity for GNP-incorporated specimens at different normal loads

dispersive spectroscopy (EDS) analysis of the worn surfaces. Some selected worn surfaces are shown in Fig. 12. As it is evident in the Fig. 12a-c, there are some dark and bright areas on the worn surfaces. The EDS analyses, Fig. 12d-g, show that the dark areas consist more carbon content, as a sign of GNPs, in comparison with the bright areas. It can be stated based on the FESEM images that the dark areas were extended, as a symptom of forming a self-lubricating

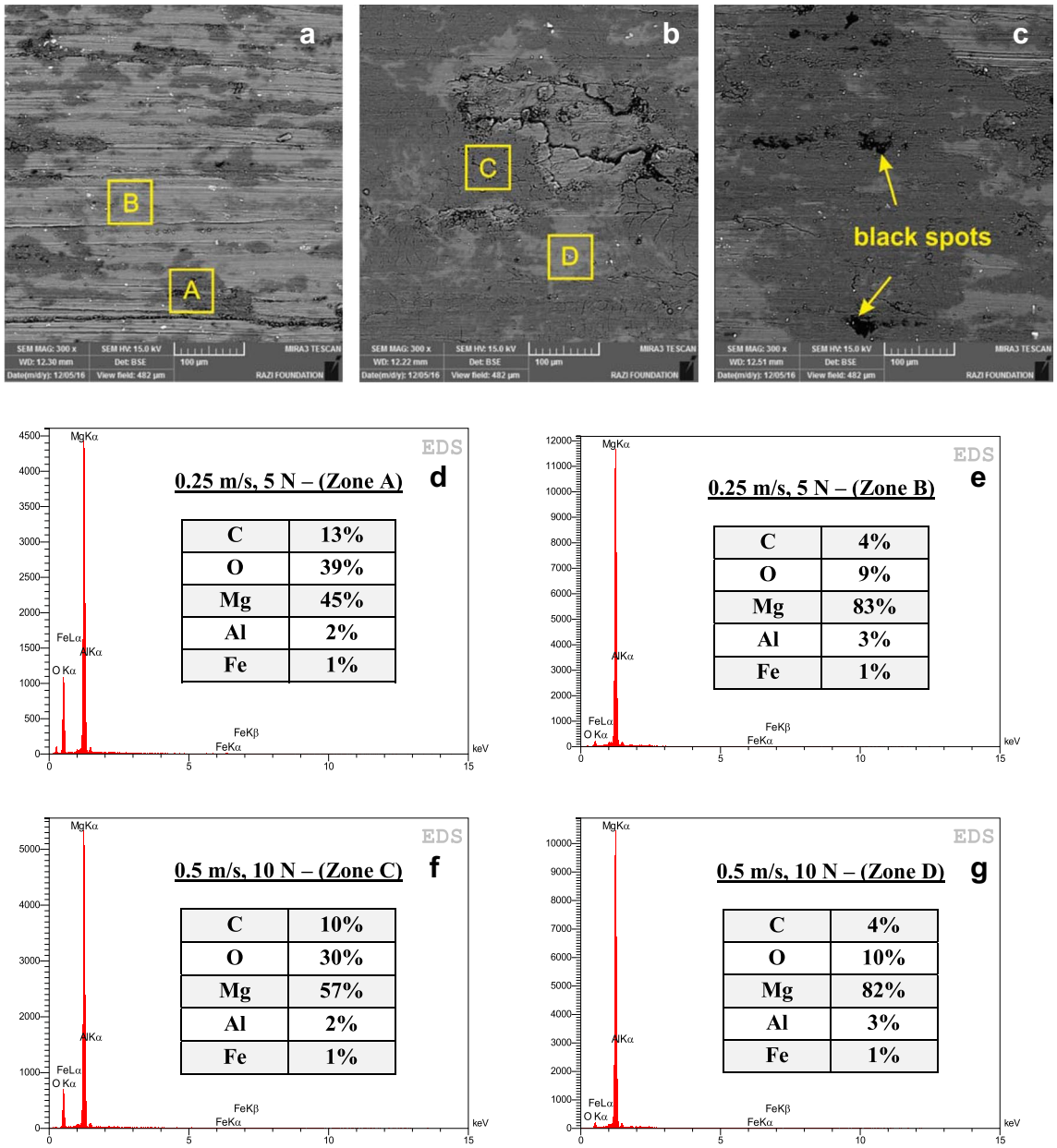

Fig. 12 FESEM microimages of some selected worn surface of GNP-incorporated specimens at 5 N and 0.25 m/s (**a**), 10 N and 0.5 m/s (**b**) and 20 N and 1.25 m/s (**c**) normal load and sliding velocity, respectively. EDS analyses of the selected areas of A (**d**), B (**e**), C (**f**) and D (**g**)

protective layer between contacting surfaces, as the normal load and sliding velocity were increased. This layer decreases adhesion and fluctuations by reducing the adhesive contact between sliding surfaces. The second effect is revealed by the morphology of GNPs in wear debris. The presence of deformed GNPs in wear debris indicates that they carry a significant portion of normal load and heat. Accordingly, the interacting surfaces are subjected to lower normal load which may be the other reason for less importance of adhesive wear mechanism and fewer value of COF for GNP-incorporated specimens. By an increase in the value of normal load, the effect of this phenomenon on the improvement of wear resistance is more evident. In fact, adding the GNPs into Mg matrix increases load-carrying capacity of the nanocomposite and improves wear resistance.

It can be observed from Fig. 11 that the lowest COF value corresponds to the highest normal load and sliding velocity. At each level of normal load, the COF value has a descending trend by increasing the sliding velocity which is more remarkable at 20 N normal load. At constant sliding velocity of 0.2 m/s, the COF value is decreased by increasing the normal load, mentioned in Table 4. The same trend also

governs on the variations of the COF value at other sliding velocities of 0.5 and 1.25 m/s.

Higher COF value at lower sliding velocity may be attributed to more damages resulted via abrasive wear mechanism by wear debris particles. In fact, metal debris particles may be entrapped between the interacting surfaces that cause abrasion. These particles are embedded into the Mg due to its softness and act like sand paper that scratches the opposite surface. This makes the worn surface much rougher, and as a result causes further wear damages. In this type of wear mechanism, the sliding surfaces exhibit different types of scratches as a function of the abrasion mode. An increase in the normal load and sliding velocity results in higher local frictional heat which facilitates the oxidative wear mechanism. Accordingly, an increase in oxidation is probably the other reason for reducing the importance of adhesion, and as a result decreasing the COF value.

As shown in Fig. 12, the dark areas are extended by an increase in the normal load and sliding velocity. The EDS analysis shows an increase in the percentage of oxygen and carbon, as a sign of GNPs, in the dark areas compared to the bright areas. As shown in Fig. 12d, e, 13% C and 39% O in the dark area (zone A) and 4% C and 9% O in the bright area (zone B) are detected at 5 N normal load and 0.2 m/s sliding velocity. Moreover, for 10 N normal load and 0.5 m/s sliding velocity, the dark area (zone C) contains 10% C and 30% O and the bright area (zone D) contains 4% C and 10% O, shown in Fig. 12f, g. It is interesting to note that carbon and oxygen contents in dark areas are almost 2–3 and 3–5 times, respectively, more than those of the bright areas. Accordingly, the lubricant layer of GNPs and the oxide surface increase the resistance against adhesive and abrasive wear. Wear resistance was improved by increasing normal load and sliding velocity. This condition also decreases both the fluctuations and the value of COF.

The different wear rate in dark and bright areas is a symptom of the lubricating effect of GNPs during sliding. The GNPs existing in the subsurface layer of nanocomposite were squeezed out to the surface during sliding. The squeezed GNPs, as well as the present GNPs on the surface, smudge onto the surface of composite. Figure 13 shows a schematic illustration of squeezing out and smudging the GNPs on the surface of nanocomposite. According to Fig. 13, applied force on the surface of nanocomposite during the wear test causes the GNPs to squeeze out, and then smudge on the surface. Actually, this phenomenon results in the formation of the above-mentioned dark areas on the worn surface, demonstrated in Fig. 12. The extent of dark areas, i.e., the amount of GNPs smudged on the surface, is likely associated with circumferential conditions such as applied force in wear test, characteristics of both the Mg alloy matrix and GNPs, and more importantly, the bonding between the matrix and reinforcement in interface [32].

Moving the GNPs to the sliding surface does not need considerable force due to the weak mechanical and chemical bonding in the interface [33, 34]. The weaker bonding between matrix and GNPs is, the easier it debonds. Furthermore, the dark areas on the worn surface were expanded by an increase in the applied force through increasing the normal load and sliding velocity during wear test. The GNPs have a planar, few layered morphology consisting of a hexagonal arrangement of carbon atoms with 0.142-nm distance between the carbon atoms in individual layers and 0.335-nm distance between planes [35]. Weak van der Waals bonding between graphene layers allows these layers to be easily separated or to slide past each other. Therefore, it can be acclaimed that the lamellar morphology of GNPs is the other contributing factor which leads to less wear rate and damages of the surface of nanocomposite.

Black spots on the worn surface, shown in Fig. 12c, are accumulations of GNPs which are increased by increasing the normal load and sliding velocity. The formation of oxidant compounds, indicated by high percentage of oxygen in dark areas, reduces the flexibility of the nanocomposite in comparison with the BM. This is one of the possible reasons for observing small cracks in these areas as can be seen in Fig. 12b, c.

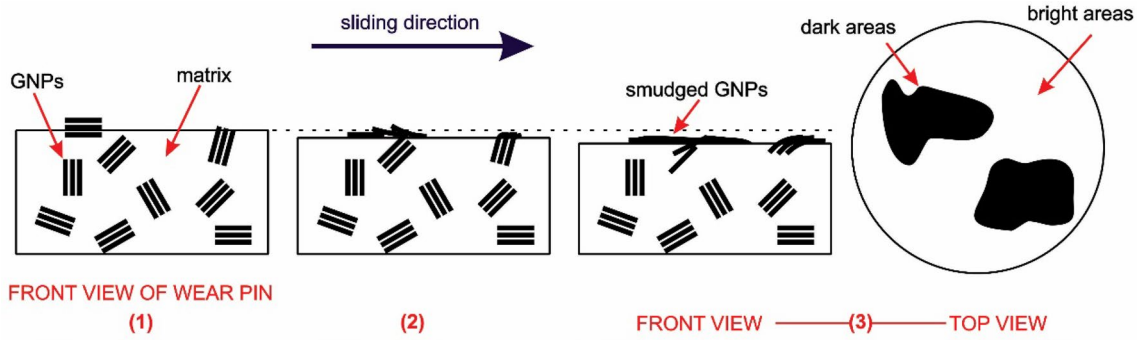

Fig. 13 Schematic illustration of the GNPs squeezed out and smudged to the surface of nanocomposite, i.e., GNP-incorporated specimen

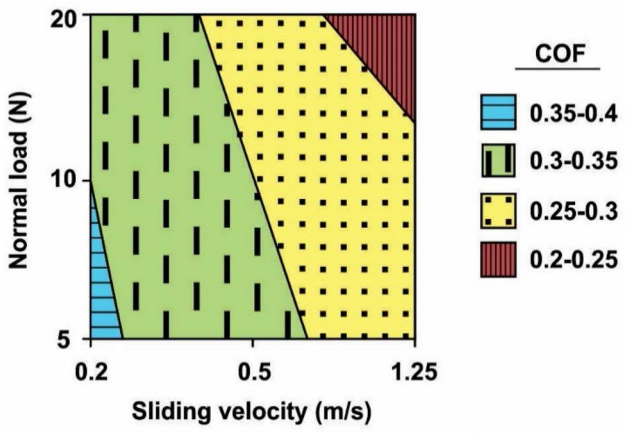

Fig. 14 Contour plot showing COF values of GNP-incorporated specimens for all investigated parameters

The cracks are expanded by increasing the normal load and sliding velocity. An Increase in the normal load and sliding velocity can intensify fatigue phenomenon which induces surface and subsurface cracks. This condition leads to the separation of larger layers from the specimen's surface and subsequently increases the intensity of delamination wear mechanism. Repeated rubbing of the debris may result in the generation of subsurface cracks, while, at some parts, inhomogeneity or imperfection leads to subsurface-initiated fatigue wear mechanism [36]. Ultimately, the subsurface cracks reach the surface and result in the removal of the material as debris, the phenomenon commonly known as delamination. Therefore, the delamination is increased by increasing the normal load and sliding velocity [36].

To elucidate the simultaneous effects of the normal load and sliding velocity, a contour plot showing variations of COF with respect to both parameters is represented in Fig. 14. This figure demarcates different regions with variations of COF elegantly. The maximum COF value corresponds to the minimum normal load and sliding velocity (horizontally lined area). It shows that the COF values are decreased by increasing the normal load and sliding velocity (dotted and dashed areas). Finally, the maximum normal load and sliding velocity result in the least value of COF in this study (vertically lined area). This indicates that different wear mechanisms are operated at different sets of the normal loads and sliding velocities.

Another reason for the foregoing trend in Fig. 14 is the effect of GNPs. Indeed, the effect of GNPs on wear resistance is more noticeable at higher normal loads and sliding velocities. This trend is consistent with the schematic illustration, shown in Fig. 13, in which the GNPs squeeze out and smudge to the surface of nanocomposite. Hence, an increase in the GNPs content leads to larger dark areas on the worn surface and, as a result, improvement of wear resistance and reduction in the COF value.

4 Conclusion

Mechanical and tribological properties of the AZ31/GNPs Mg composite, fabricated by FSP, were investigated. The brief conclusion about the findings is as follows:

1. Equiaxed and fully recrystallized microstructure with a range of 3–9 μm grain size was discovered. Refined microstructure and the presence of GNPs increased the microhardness by around 41%.
2. Conventional FSP specimen showed 133% increase in strain-to-fail, while it was decreased by adding GNPs. However, the presence of GNPs increased the YS and UTS to 217 and 278 MPa, respectively.
3. Adding GNPs not only caused around 60% decrease in the COF value, but also resulted in confined range of fluctuations in friction plot.
4. An increase in the normal load and sliding velocity resulted in more expansion of the dark areas, covered by GNPs, due to easier interfacial failure between the GNPs and the surrounding AZ31 Mg matrix.
5. Applied force causes the GNPs to squeeze out, and then smudge on the surface which results in the formation of some dark areas on the worn surface. An increase in the dark areas leads to fewer wear rate and damages.
6. The GNPs carried significant portion of normal load, and subsequently, they reduced the importance of adhesive wear and diminished the COF value in nanocomposites.
7. An increase in the normal load and sliding velocity reduced the intensity of adhesive and abrasive wear damages and increased the oxidation and small surface and subsurface micro-cracks.
8. The contour plot showed that the maximum COF value corresponds to the minimum normal load and sliding velocity. It was decreased by increasing the normal load and sliding velocity.

Compliance with Ethical Standards

Conflict of interest The authors declare that they have no conflict of interest.

References

1. Pol, V.G., Thackeray, M.M., Mistry, K., Erdemir, A.: Novel materials as additives for advanced lubrication. Google Patents (2014)
2. Ren, L., Fan, L., Zhou, M., Guo, Y., Zhang, Y., Boehlert, C.J., et al.: Magnesium application in railway rolling stocks: a new challenge and opportunity for lightweighting. Int. J. Lightweight Mater. Manuf. (2018)
3. Suneesh, E., Sivapragash, M.: Comprehensive studies on processing and characterization of hybrid magnesium composites. Mater. Manuf. Processes **33**, 1324–1345 (2018)
4. Wu, L., Wu, R., Hou, L., Zhang, J., Zhang, M.: Microstructure, mechanical properties and wear performance of AZ31 matrix composites reinforced by graphene nanoplatelets (GNPs). J. Alloy. Compd. **750**, 530–536 (2018)
5. Turan, M.E., Sun, Y., Aydin, F., Zengin, H., Turen, Y., Ahlatci, H.: Effects of carbonaceous reinforcements on microstructure and corrosion properties of magnesium matrix composites. Mater. Chem. Phys. (2018)
6. Novoselov, K.S., Geim, A.K., Morozov, S., Jiang, D., Zhang, Y., Dubonos, S.a., et al.: Electric field effect in atomically thin carbon films. Science **306**, 666–669 (2004)
7. Moghadam, A.D., Omrani, E., Menezes, P.L., Rohatgi, P.K.: Mechanical and tribological properties of self-lubricating metal matrix nanocomposites reinforced by carbon nanotubes (CNTs) and graphene–a review. Compos Part B **77**, 402–420 (2015)
8. Ling, W.D., Wei, P., Duan, J.Z., Chen, J.M., Duan, W.S.: First-principles study of the friction and wear resistance of graphene sheets. Tribol. Lett. **65**, 53 (2017)
9. Lee, C., Wei, X., Kysar, J.W., Hone, J.: Measurement of the elastic properties and intrinsic strength of monolayer graphene. Science **321**, 385–388 (2008)
10. Moghadam, A.D., Schultz, B.F., Ferguson, J., Omrani, E., Rohatgi, P.K.: Gupta, N. Functional metal matrix composites: self-lubricating, self-healing, and nanocomposites-an outlook. JOM **66**, 872–881 (2014)
11. Berman, D., Erdemir, A., Sumant, A.V.: Graphene: a new emerging lubricant. Mater. Today **17**, 31–42 (2014)
12. Gerlich, A.P.: Critical assessment: friction stir processing, potential, and problems. Mater. Sci. Technol. **33**, 1139–1144 (2017)
13. Ceschini, L., Dahle, A., Gupta, M., Jarfors, A.E.W., Jayalakshmi, S., Morri, A., et al.: Aluminum and magnesium metal matrix nanocomposites. Springer, Berlin (2017)
14. Hu, Z., Tong, G., Lin, D., Chen, C., Guo, H., Xu, J., et al.: Graphene-reinforced metal matrix nanocomposites–a review. Mater. Sci. Technol. **32**, 930–953 (2016)
15. Chen, L.-Y., Konishi, H., Fehrenbacher, A., Ma, C., Xu, J.-Q., Choi, H., et al.: Novel nanoprocessing route for bulk graphene nanoplatelets reinforced metal matrix nanocomposites. Scripta Mater. **67**, 29–32 (2012)
16. Rashad, M., Pan, F., Tang, A., Lu, Y., Asif, M., Hussain, S., et al.: Effect of graphene nanoplatelets (GNPs) addition on strength and ductility of magnesium-titanium alloys. J. Magnes. Alloys **1**, 242–248 (2013)
17. Rashad, M., Pan, F., Tang, A., Asif, M., She, J., Gou, J., et al.: Development of magnesium-graphene nanoplatelets composite. J. Compos. Mater. **49**, 285–293 (2015)
18. Rashad, M., Pan, F., Asif, M., Tang, A.: Powder metallurgy of Mg–1% Al–1% Sn alloy reinforced with low content of graphene nanoplatelets (GNPs). J. Ind. Eng. Chem. **20**, 4250–4255 (2014)
19. Sigma-Aldrich, Corporate Offices, S.A., 3050 Spruce St., St. Louis, MO 63103. https://xgsciences.com/materials/graphene-nano-platelets/. Accessed 1 Jan (2016)
20. Standard, A.: E3-11, 2011,"Standard Guide for Preparation of Metallographic Specimens", ASTM International, West Conshohocken, https://doi.org/10.1520/E0003-11. (2017)
21. Testing, A.S.f.: Materials: ASTM E112-96 (2004) e2: Standard test methods for determining average grain size. ASTM, West Conshohocken (2004)
22. International, A.: ASTM E384-99-Standard Test Method for microindentation hardness of materials. ASTM International, West Conshohocken (1999)
23. Standard, A.: G99, Standard Test Method for Wear Testing with a Pin-on-Disk Apparatus. ASTM International, West Conshohocken (2006)
24. Faraji, G., Asadi, P.: Characterization of AZ91/alumina nanocomposite produced by FSP. Mater. Sci. Eng. A **528**, 2431–2440 (2011)
25. Darras, B., Kishta, E.: Submerged friction stir processing of AZ31 Magnesium alloy. Mater. Des. **47**, 133–137 (2013)
26. Rashad, M., Pan, F., Asif, M.: Magnesium matrix composites reinforced with graphene nanoplatelets. Gr. Mater. (2015). https://doi.org/10.1002/9781119131816.ch5
27. Arsenault, R., Shi, N.: Dislocation generation due to differences between the coefficients of thermal expansion. Mater. Sci. Eng. **81**, 175–187 (1986)
28. Rashad, M., Pan, F., Hu, H., Asif, M., Hussain, S., She, J.: Enhanced tensile properties of magnesium composites reinforced with graphene nanoplatelets. Mater. Sci. Eng. A **630**, 36–44 (2015)
29. Zahmatkesh, B., Enayati, M.: A novel approach for development of surface nanocomposite by friction stir processing. Mater. Sci. Eng. A **527**, 6734–6740 (2010)
30. Asadi, P., Faraji, G., Masoumi, A., Givi, M.B.: Experimental investigation of magnesium-base nanocomposite produced by friction stir processing: effects of particle types and number of friction stir processing passes. Metal. Mater. Trans. A **42**, 2820–2832 (2011)
31. An, J., Li, R., Lu, Y., Chen, C., Xu, Y., Chen, X., et al.: Dry sliding wear behavior of magnesium alloys. Wear **265**, 97–104 (2008)
32. Sarmadi, H., Kokabi, A., Reihani, S.S.: Friction and wear performance of copper–graphite surface composites fabricated by friction stir processing (FSP). Wear **304**, 1–12 (2013)
33. Kováčik, J., Emmer, Š, Bielek, J.: Effect of composition on friction coefficient of Cu–graphite composites. Wear **265**, 417–421 (2008)
34. Kim, J., Kestursatya, M., Rohatgi, P.: Tribological properties of centrifugally cast copper alloy-graphite particle composite. Metal. Mater. Trans. A **31**, 1283–1293 (2000)
35. Zhen, Z., Zhu, H.: Structure and properties of graphene. Graphene, pp. 1–12. Elsevier, Amsterdam (2018)
36. Arora, H., Singh, H., Dhindaw, B.: Wear behaviour of a Mg alloy subjected to friction stir processing. Wear **303**, 65–77 (2013)